*metals*

MDPI

*Article*

# Investigating the Mechanics of Hybrid Metal Extrusion and Bonding Additive Manufacturing by FEA

**Jørgen Blindheim *, Torgeir Welo and Martin Steinert**

Department of Mechanical and Industrial Engineering, Norwegian University of Science and Technology, 7491 Trondheim, Norway

* Correspondence: jorgen.blindheim@ntnu.no; Tel.: +47-905-02-216

Received: 21 June 2019; Accepted: 18 July 2019; Published: 24 July 2019


**Abstract:** Hybrid Metal Extrusion & Bonding Additive Manufacturing (HYB-AM) is a hybrid manufacturing technology for the deposition of layered metal structures. This new deposition process is a complex metal forming operation, yet there is significant lack of knowledge regarding the governing mechanisms. In this work, we have used finite element analysis (FEA) to study material flow in the extruder, as well as the conditions at the interfaces of the deposited extrudate and the substrate, aiming to identify and characterize the process parameters involved. Analysis of the material flow shows that the extrusion pressure is virtually independent of the deposition rate. Furthermore, from the simulations of the material deposition sequence, it is clearly visible how the contact pressure at the interface will drop below the bonding threshold if the feed speed is too high relative to the material flow through the die. The reduced pressure also leads to the formation of a 'gas-pocket' inside the die, thus further degrading the conditions for bonding. The analyses of the process have provided valuable insights for the further development and industrialization of the process.

**Keywords:** additive manufacturing; conform extrusion; HYB-AM; aluminium alloys

## 1. Introduction

Hybrid Metal Extrusion and Bonding Additive Manufacturing (HYB-AM) is a new solid-state additive manufacturing process for the fabrication of layered 3D metal structures [1,2]. The process operates in the solid-state, meaning that defects associated with melting of the feedstock material are avoided. Furthermore, the low heat input enables high deposition rates when compared to the melted-state AM-process. The process is, therefore, particularly suitable for low-volume manufacturing of larger components where subtractive machining becomes inefficient due to low material utilization, or where forming or casting processes are disqualified due to high tooling costs.

In HYB-AM, the feedstock material is processed through a continuous rotary extruder, which serves the purpose of dispersing oxides and providing pressure for bonding to occur between the extrudate and the substrate. During operation, the die is scraping the substrate to remove surface oxides as the feedstock material is deposited in a stringer-by-stringer manner to form layers. The principle is illustrated in Figure 1. After deposition, the part needs to be post-processed by traditional subtractive machining to obtain the desired net-shape. The latest extruder design and samples produced by this process are shown in Figure 2.

Up until now, the research on the HYB-AM process has focused on concept development through physical modelling, along with full-scale experiments using AA6082 feedstock material, an Al-Mg-Si alloy mainly used for hot forming processes. The first full-scale experiments aimed at demonstrating

the process on a proof-of-concept level and exploring the potential of the process [3]. More recently, a full-scale experiment was carried out to assess the mechanical integrity of a deposited structure [4]. Microscopy analyses show that fully dense bonding interfaces can be achieved, though some voids can be observed between the individual stringers. Observations of fracture surfaces reveal areas of full metallic bonding; however, regions of kissing-bonds and lack of bonding are also visible. Through these full-scale experiments, the HYB-AM process has demonstrated its proof-of-concept and capability for processing advanced aluminium alloys. Nevertheless, this process is a complex metal forming operation, and the governing mechanisms need to be better understood in order to optimize the process towards industrialization.

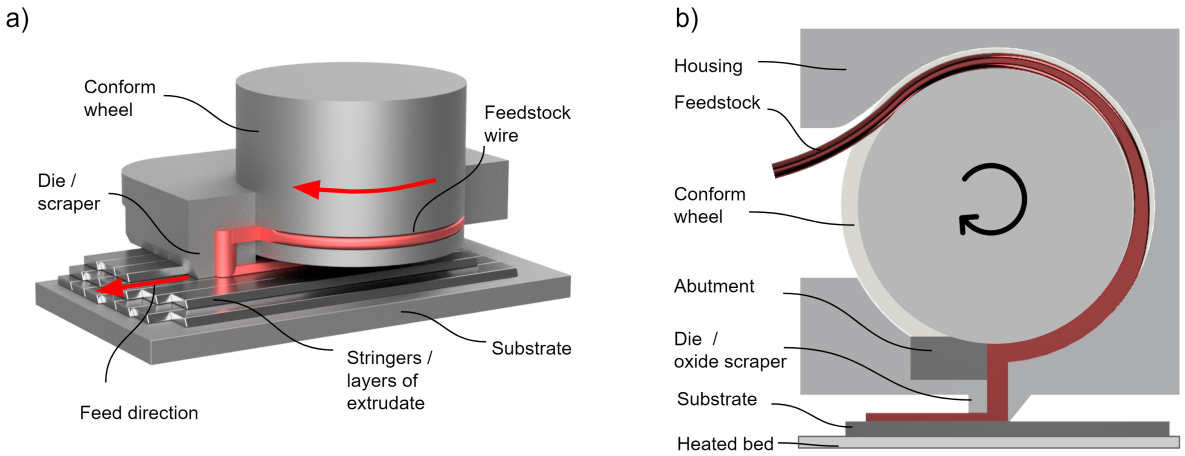


**Figure 1.** The extruder consists of a wheel with a groove surrounded by a stationary housing. The feedstock wire is pressed into the groove, and upon rotation the extrusion pressure is built up as the material is blocked by an abutment close to the die. The die also acts as a scraper in order to remove oxides from the substrate prior to bonding with the extrudate. (**a**) principal illustrations of the hybrid metal extrusion & bonding additive manufacturing (HYB-AM) extruder; (**b**) rendering of the extruder and a deposited structure.

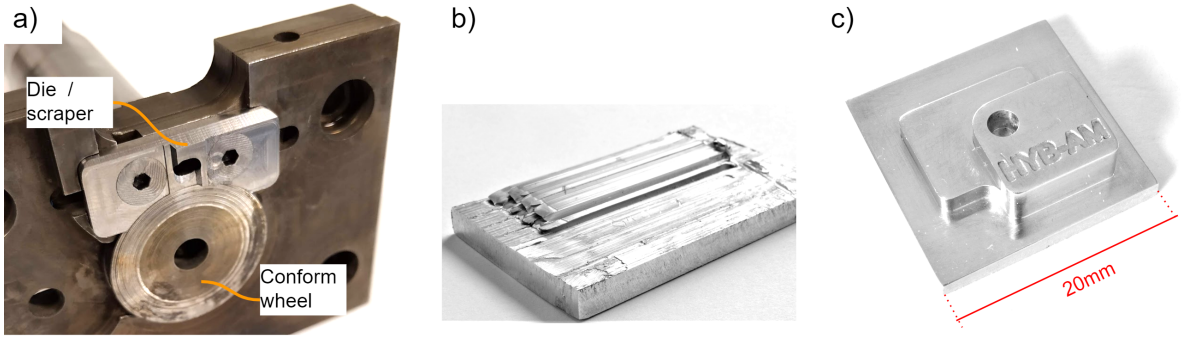


**Figure 2.** Full-scale demonstration of the HYB-AM process. (**a**) the extruder prototype; (**b**) two layers (4 + 3 stringers) of AA6082 deposited on a substrate of the same alloy; (**c**) net-shape demo sample after post-processing by subtractive machining.

In this study, we have applied finite element analysis (FEA) using commercially available Deform 3D software to analyse and interpret some of the governing mechanisms of the process. The following objectives are covered: (1) to study the material flow in the extruder with regard to extrusion grip length, contact pressure, peak temperatures and strain-rates at steady-state for two different deposition rates; (2) to investigate the thermo-mechanical conditions for the bond interface between the extrudate and the substrate with regard to the obtained contact pressure at different ratios between extrusion flow rate and feed speed.

The remainder of this paper is organized as follows: The next section provides an introduction to the working principles of the HYB-AM process. Section 3 presents the FEM-models and simulation parameters used throughout the study. Section 4 presents the results from the simulations, while Section 5 discusses the results. Conclusions are given in Section 6.

## 2. The HYB-AM Process

The pressure-generating mechanism in the HYB-AM extruder is based on the principle of continuous rotary extrusion (CRE), also known as Conform extrusion [5,6]. Over the past several decades, the CRE process has been subjected to multiple studies, covering the range of Al, Cu, Mg and Ti alloys [7–11]. More recently, as FEM-modelling has become a viable tool for this type of problems, several studies have validated the relationships between simulations and full-scale experiments. Kim et al. [12] used numerical simulation to identify optimal process parameters for CRE. Hodek and Zemko [13] studied CRE of titanium through experiments and simulations. Valberg et al. [14] have used FEA to study the early stages of CRE using aluminium feedstock, while Rajendran et al. have simulated processing of AA3003 [15] and magnesium alloy AZ91 [16].

Following the illustration in Figure 1b, the extrusion pressure is created by the frictional force between the feedstock wire and the tapered groove of the rotating wheel. The wheel is sealed by a stationary housing provided with an abutment and a die. The feedstock is firmly pressed into the groove and driven forward by the rotation of the wheel. Subsequently, the feedstock wire is blocked by the abutment and axial compression is induced, causing the material to yield and fill the entire cross-section. This, in turn, increases the contact surface and friction, leading to further pressure build-up, ultimately causing the material to flow out of the die.

Figure 1a illustrates the HYB-AM deposition sequence. A blank of aluminium is fixed on a heated bed to act as a substrate upon which the material is deposited. The extruder adds material as it moves in the direction of deposition, placing stringers side-by-side to form a layer, and allowing new layers to be added on top of each other. As deposition proceeds, the die-outlet is simultaneously scraping the underlying layer and the side wall of the adjacent stringer to remove the oxide layer. This creates the required conditions for bonding with the extrudate to occur. The metal flow and the bonding mechanisms in the HYB-AM process are similar to those observed in longitudinal seam welds of porthole-die extrusions, where welds are formed under high pressure as material streams merge after flowing around the die-bridges [17–20]. However, unlike porthole-die extrusions, in the case of HYB-AM, the merging metal streams should be considered as mating streams of extrudate and substrate.

## 3. Materials and Methods

### *3.1. FEM-Models*

The CAD files for the FEM-models were prepared in Fusion 360 (V2.0, Autodesk, San Rafael, CA, USA). The overall design is similar to that of the parts used for the full-scale experiments (Figure 2), except for the geometry being modified such that an interference is added between all moving parts to prevent loss of nodes during simulations. The FEM analysis is conducted in Deform 3D software (V11.3, Scientific Forming Technologies Corporation, Columbus, OH, USA).

Full-scale experiments on the HYB-AM process have been conducted on AA6082 feedstock material. For the FEM-analysis, the flow stress data for AA6082, as a function of strain and temperature for various strain rates, were obtained from the material library in the software, which is based on [21]. Figure 3 presents the flow stress curves for the temperature range 300 °C to 500 °C for strain rates of 0.3 $s^{-1}$, 10 $s^{-1}$and 100 $s^{-1}$.

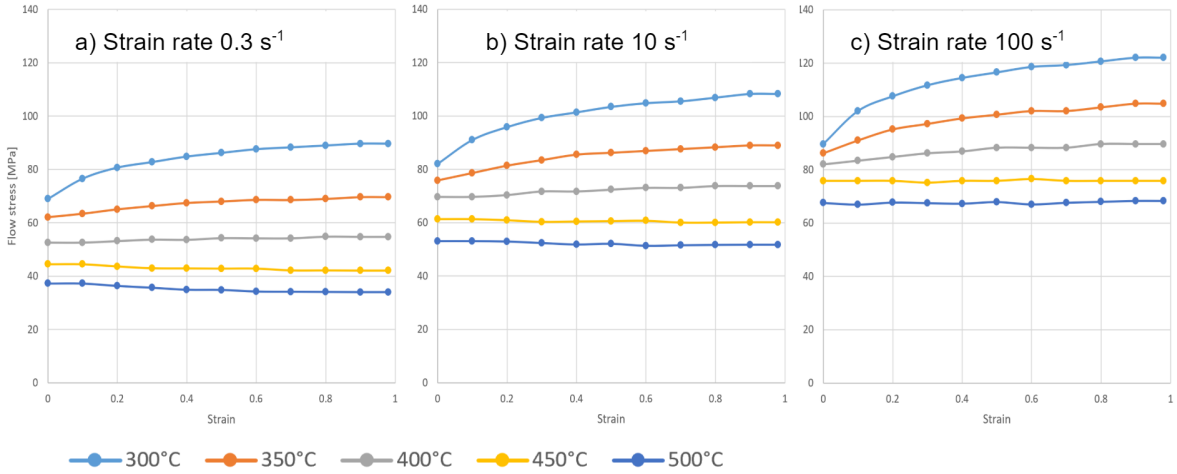


**Figure 3.** Material data for AA6082 at in the range 300°C to 500°C for strain rates: (**a**) $0.3s^{-1}$, (**b**) $0.3s^{-1}$ and (**c**) $100s^{-1}$. Data is obtained from Deform 3D material library based on [21].

### *3.2. Model 1: Extrusion Pressure Generating Mechanism*

The numerical model of the extruder consists of the housing, the conform wheel and the feedstock material, as depicted in Figure 4. The abutment and the die geometry is merged with the housing to simplify meshing of the FEM-model.

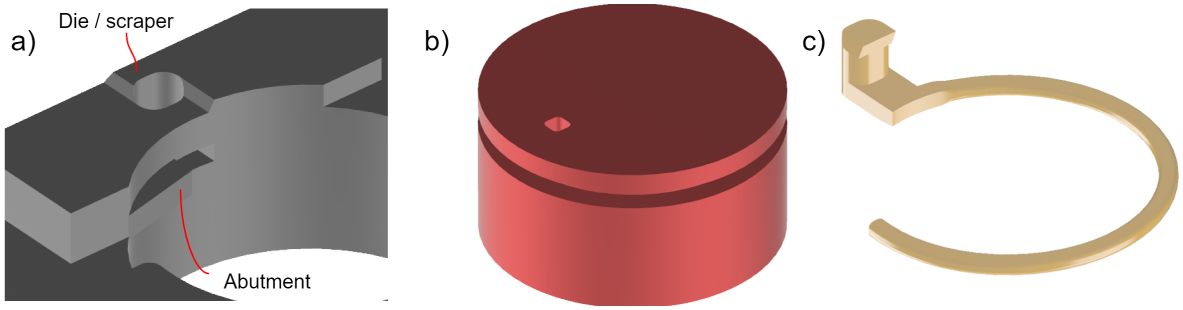


**Figure 4.** The geometry used for finite element method (FEM) model 1 as seen from below. (**a**) the housing, merged with the die and the abutment; (**b**) the conform wheel; (**c**) the feedstock wire.

Referring to the first objective (1), our investigations aim to observe the material flow at steady-state conditions. The simulations were, therefore, initiated with a filled chamber and die, but with the extrusion grip length shorter than what expected to be seen at steady-state. The feedstock wire is partially formed to the shape of the groove in the wheel, yet it has the same cross-section as that of the Ø1.6 mm feedstock wire, see Figure 5a. The surface area in contact with the groove walls and the wall of the housing is shown in Figure 5b. A rigid surface is modeled to represent the substrate at the die outlet in order to obtain extrusion pressures at the same magnitude as that achieved during deposition.

Two different simulations have been carried out for model 1, where the angular velocity of the wheel is the only parameter subjected to change. The Tresca friction model is used for modelling contact friction; $\tau = m \cdot k$, [22], where $\tau$ is the frictional stress, $m$ is the friction factor and $k$ is the shear yield stress. The friction factor between the feedstock material and the tooling was kept arbitrary high, $m = 2$, to ensure sticking friction condition with no sliding. The feedstock is modelled as a rigid-plastic material and the tooling is modelled as a rigid surface. A heat transfer coefficient of 11(N/s)/(mm/c) is applied for the contact between the feedstock and the tool parts. The meshes are shown in Figure 6 and the complete set of simulation parameters can be found in Table 1.

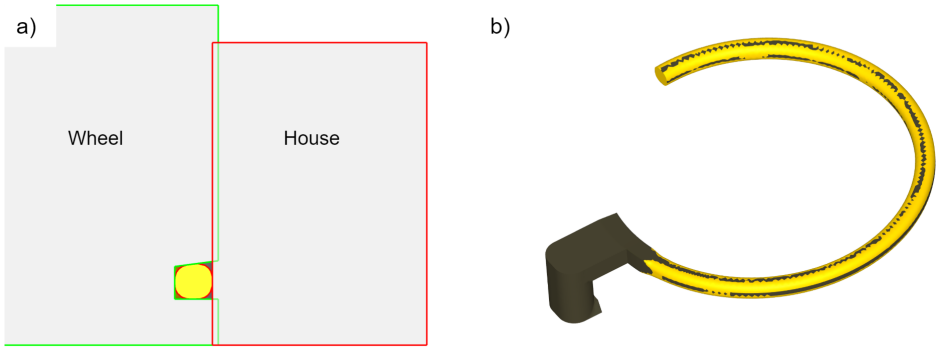


**Figure 5.** The initial contact between the feedstock material and the tooling for model 1. (**a**) section through the wheel and housing; (**b**) the feedstock with indication of contact points.

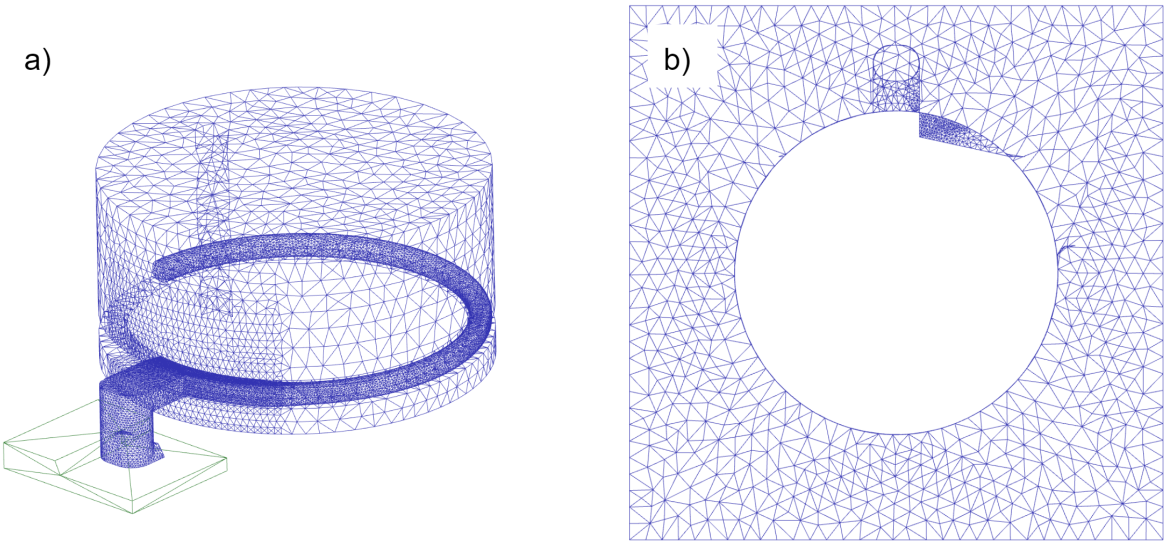


**Figure 6.** The meshes used for model 1. The meshes are refined in the plastic zone where the strain rates are at the highest. (**a**) the wheel and the feedstock material; (**b**) the housing.

### *3.3. Model 2: Stringer Deposition Sequence*

A separate model has been made to study the material flow and normal pressure at the interface between the die outlet and the substrate. In this model, both the substrate and the feedstock are modelled using a rigid-plastic material representation. The components used in this model are shown in Figure 7, and the simulation parameters are listed in Table 2. The material supply in this model is simplified by the direct extrusion principle where a billet of feedstock is placed in a container and a ram is used to generate the material flow. The substrate model resembles the shape of multiple preceding layers and some stringers of the current layer. The substrate is fixed on a rigid bed, which can move along the feed axis. For the two simulations carried out for model 2, the feed speed is kept constant while the speed of the ram is altered.

**Table 1.** Parameters used in finite element method (FEM)-model 1.

| Parameter | Parameter | Value |
|---|---|---|
| General | Pin diameter | 28 mm |
| | Feedstock wire diameter | 1.6 mm |
| | Heat transfer coefficient feedstock/tooling | 11(N/s)/(mm/c) |
| | Simulation type | Lagrangian Deformation & Heat transfer |
| | Mesh type | Tetrahedral |
| House | Initial temperature | 300 °C |
| | Material | AISI-H13 |
| | Friction factor against feedstock, m | 2 |
| | Initial mesh elements/nodes | 48,031/10,844 |
| | Mesh refinement in plastic zone | 0.07 |
| | Mesh refinement die | 0.25 |
| Wheel | Initial temperature | 300 °C |
| | Material | AISI-H13 |
| | Friction factor against feedstock, m | 2 |
| | Initial mesh elements/nodes | 29,690/6734 |
| | Mesh refinement in plastic zone | 0.1 |
| | Rotational speed | 4 RPM/50 RPM |
| Feedstock | Initial temperature | 300 °C |
| | Material | AA6082 |
| | Initial mesh elements/nodes | 124,837/28,375 |
| | Mesh refinement in plastic zone | 0.5 |
| | Friction factor against feedstock, m | 2 |
| Substrate | Initial temperature | 300 °C |
| | Material | AISI-H13 |
| | Friction factor against feedstock, m | 0 |

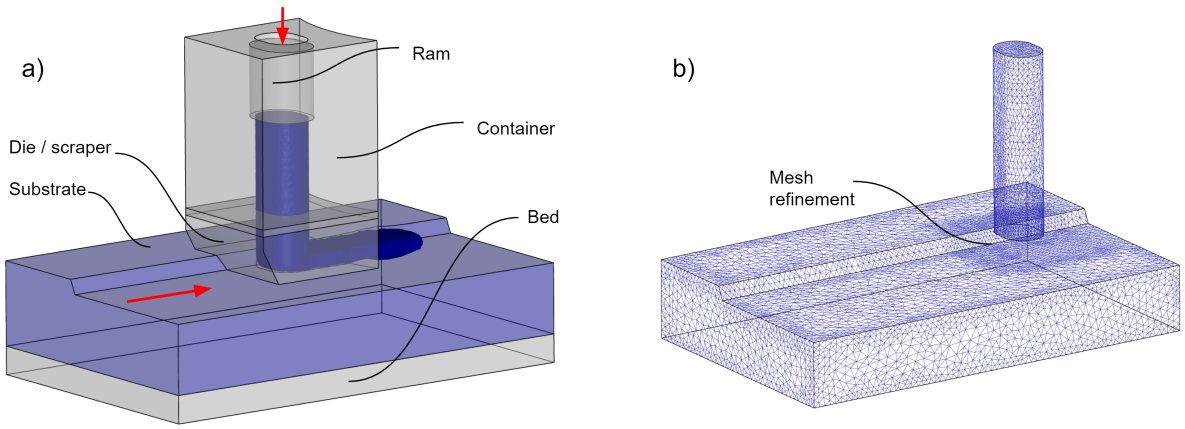


**Figure 7.** FEM model 2. (**a**) the material deposition is controlled by the ram speed and the horizontal movement of the substrate; (**b**) the initial mesh of the feedstock and the substrate with mesh refinement at the joining interface.

**Table 2.** Parameters used in FEM-model 2.

| Parameter | Parameter | Value |
|---|---|---|
| General | Simulation type | Lagrangian Deformation |
| | Mesh type | Tetrahedral |
| Feedstock | Material | AA6082 |
| | Temperature | 500 °C |
| | Initial mesh elements/nodes | 33,261/7379 |
| | Mesh refinement | 0.2 |
| Substrate | Material | AA6082 |
| | Temperature | 500 °C |
| | Initial mesh elements/nodes | 79,710/17,714 |
| | Mesh refinement | 0.35 |
| | Contact condition feedstock | non-separable |
| | Friction factor against feedstock, m | 2 |
| Die | Friction factor against feedstock, m | 2 |
| | Friction factor substrate, m | 0 |
| | Inlet cross-section area | 10.5 $mm^2$ |
| | Outlet cross-section area | 3.5 $mm^2$ |
| Ram | Speed, Balanced/High | 1.0/1.2 mm/s |
| Container | Friction factor against feedstock, m | 0 |
| Bed | Friction factor substrate, m | 2 |
| | Feed delay | 1 s |
| | Speed in feed direction | 3.0 mm/s |

## 4. Results

### *4.1. Model 1*

Simulations for model 1 have been carried out at two different rotational speeds of the extruder, 4 RPM and 50 RPM, where the former being the setting used for prior full-scale experiments [4].

Figure 8 shows the length of the extrusion grip zone for the initial condition (a) and for steady-state for the two rotational speeds considered in the study (b and c). In the primary grip zone of CRE, the wire should be firmly fixed in the groove in order to induce compressive stresses, leading to upsetting of the material and thus establishment of the extrusion grip zone. Despite the difference in rotational speed, the extrusion grip lengths are of the same magnitude for Figure 8b,c. Figure 9 shows the total velocity of the feedstock material and the wheel, confirming that the wire has the same velocity as the wheel in the primary grip zone.

A contour plot of the strain-rates is shown in Figure 10 for both rotational speeds subjected to analysis. At 50 RPM, the flow stress is expected to increase due to the increased strain-rates; however, the temperature also increases, as depicted in Figure 11. It is observed that at 4 RPM the temperature peaks at 330 °C, while at 50 RPM the temperature reaches 550 °C.

Figure 12 illustrates the contact pressure between the feedstock material and the walls of the groove and the housing. For both rotational speeds, the contact pressure is at the same level, despite the difference in flow rate.

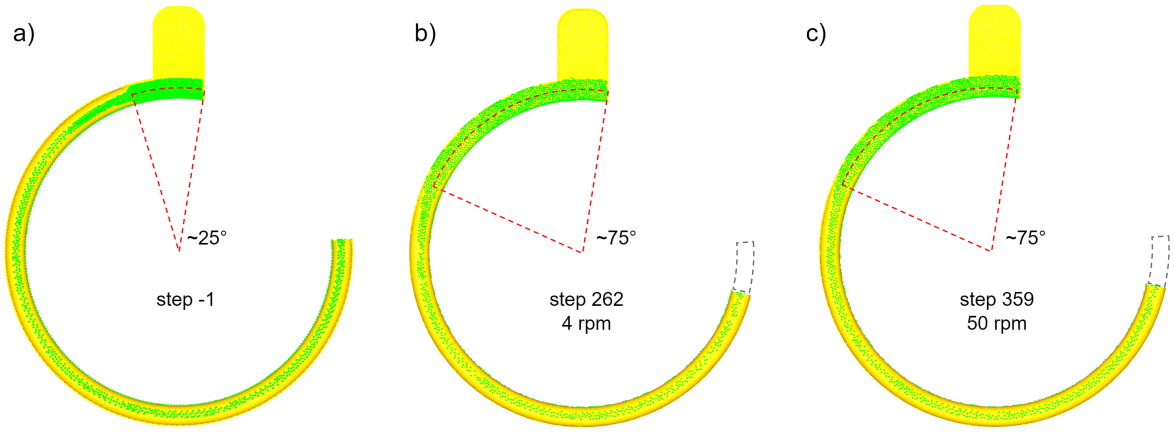


**Figure 8.** The feedstock material and the nodal contact points at steady-state for different rotational speeds. (**a**) the initial extrusion grip length in the extruder; (**b**) extrusion grip length at 4 RPM; (**c**) extrusion grip length at 50 RPM is similar to that of 4 RPM.

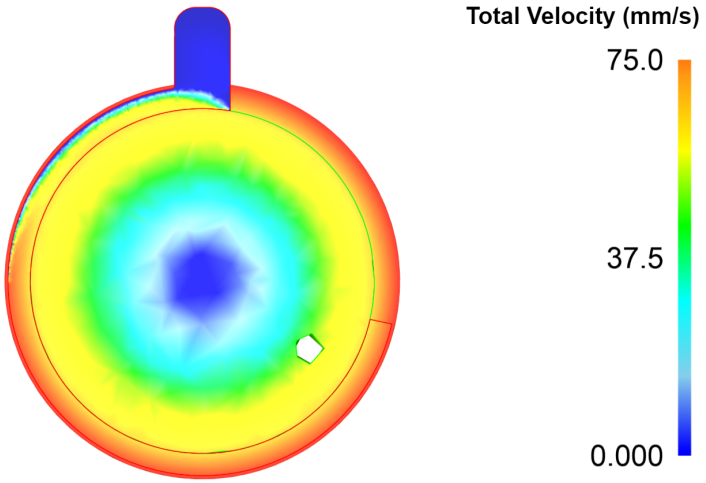


**Figure 9.** Section through the groove of the conform wheel displaying maximum element velocity at 50 RPM. The feedstock wire has the same velocity as the wheel in the primary grip zone. In the extrusion grip zone, the feedstock is stationary as it sticks to the wall of the housing, whereas at the inner wall of the groove the material has the velocity of the wheel.

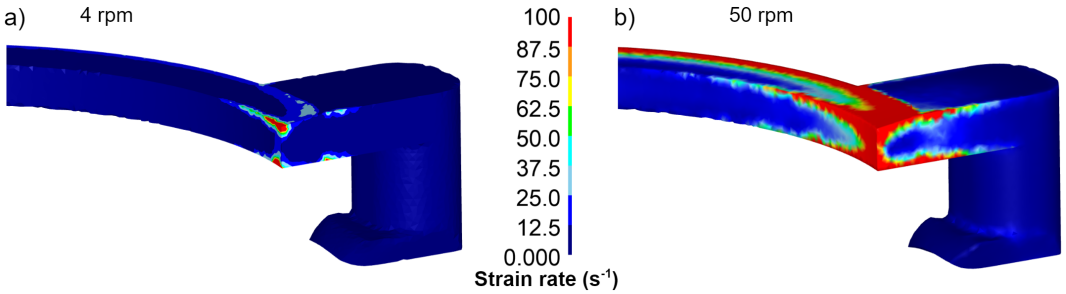


**Figure 10.** Strain rates in the extrusion grip zone. (**a**) rotational speed 4 RPM; (**b**) rotational speed 50 RPM.

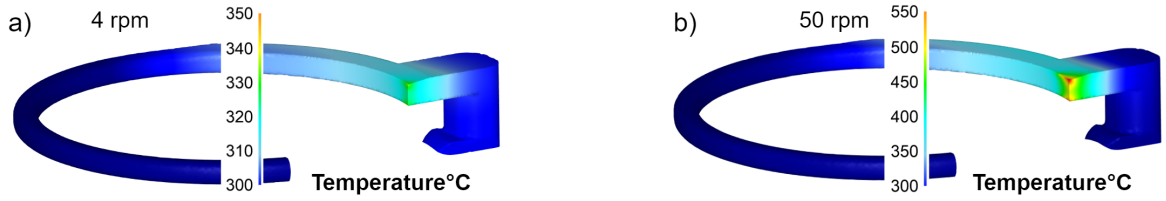


**Figure 11.** Temperature level in the extrusion grip zone. (**a**) rotational speed 4 RPM; (**b**) rotational speed 50 RPM.

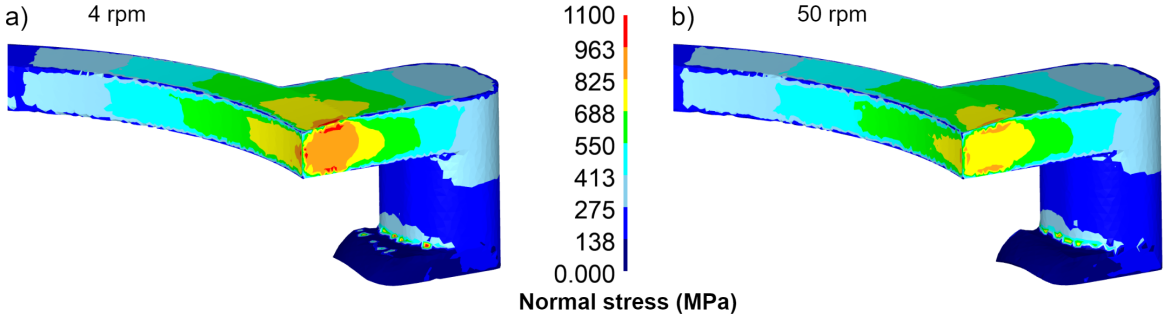


**Figure 12.** Normal pressure in the extrusion grip zone. (**a**) rotational speed 4 RPM; (**b**) rotational speed 50 RPM.

### *4.2. Model 2*

The only parameter subjected to change in model 2 is the ratio between the ram speed and the feed speed. At a balanced ratio, the volumetric flows at both the inlet and the outlet (the rear opening between the substrate and the die) are equal, whereas at high speed the inlet flow is increased by 20% through increased ram speed. In the simulations, the ram is moved for one second to have the extrudate fill the die cavity prior to moving the bed.

Figure 13 illustrates the effective stress for the balanced and high ratios of ram vs. feed speed, respectively. For the balanced ratio, it can be seen that after 1.2 s the section of the die cavity is completely filled (Figure 13a). However, as deposition proceeds, a pocket is formed in the front part of the die (Figure 13b). For the high ratio (Figure 13c,d), the plastic region of the substrate is higher than for the balanced ratio after 1.2 s, and the stress levels have further increased after 5 s.

For solid-state bonding to occur in the absence of surface oxides, the normal stress at the bonding interface must exceed the instantaneous flow stress of the material. Referring to Figure 14, the strain rate of the extrudate in contact with the substrate is in the range of 0 to 7 $s^{-1}$. For the actual temperatures and strain rates, the flow stress of the material is less than 50 MPa (Figure 3). When adding a margin of 10%, the bonding threshold can be estimated to 55 MPa.

Figure 15 illustrates the normal stress in a section through the die, perpendicular to the deposition direction. For the balanced speed ratio, the normal stresses exceed 55 MPa only in the centre part of the die, whereas, for the high ratio, the full width of the stringer is subjected to contact stresses above the estimated bonding threshold.

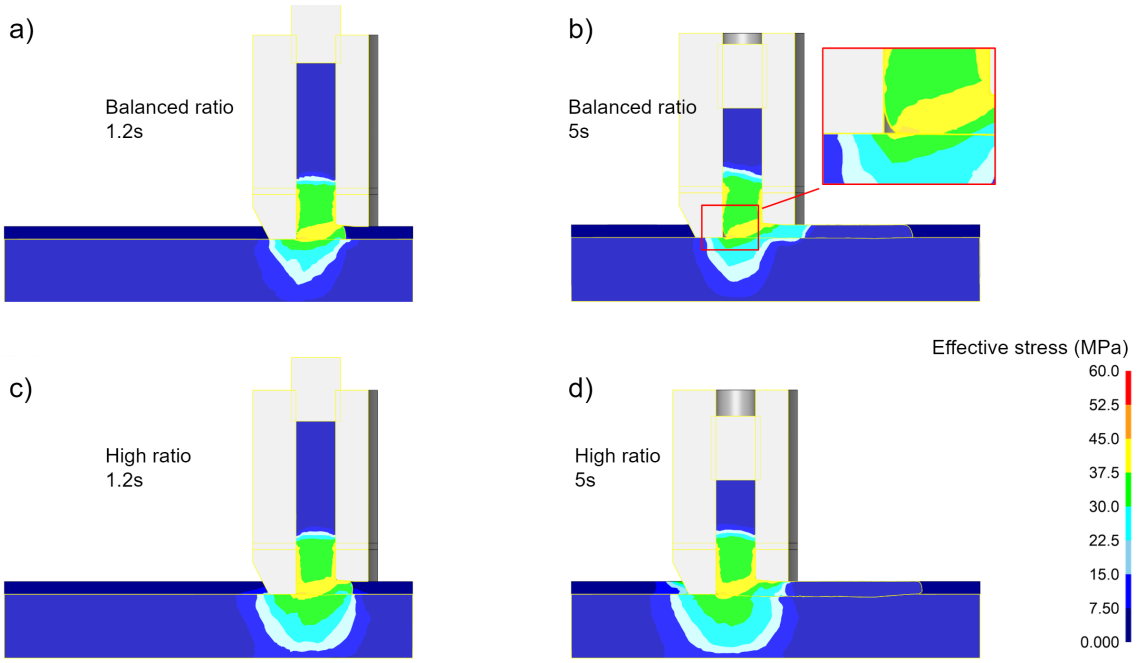


**Figure 13.** Effective stress during deposition at 500 °C. (**a**) balanced ratio; after 1.2 s the die cavity is filled and the feeding has started; (**b**) balanced ratio; after 5 s a pocket is formed in the front section of the die; (**c**) high ratio; after 1.2 s, the die cavity is filled; (**d**) high ratio; after 5 s, the die cavity is still full and the effective stress has increased.

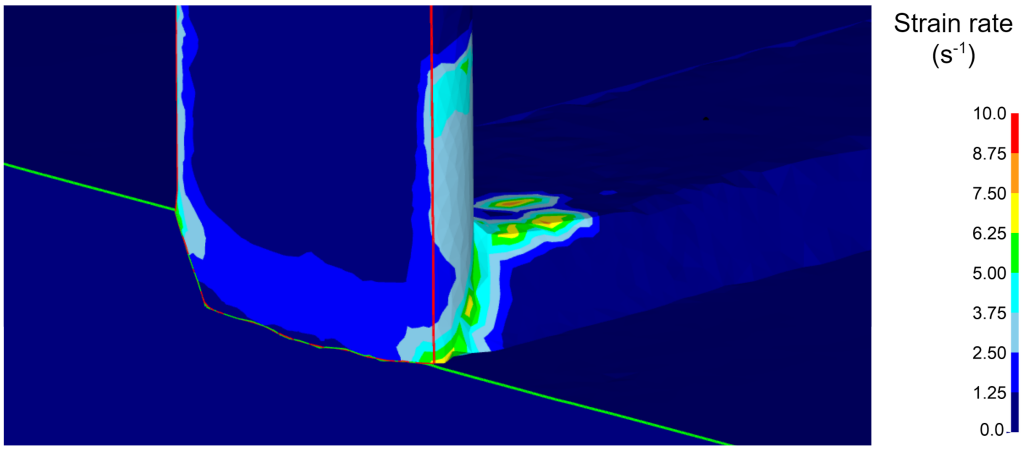


**Figure 14.** Strain rate at the bonding interface. The strain rates are in the range of 0 to 7 $s^{-1}$.

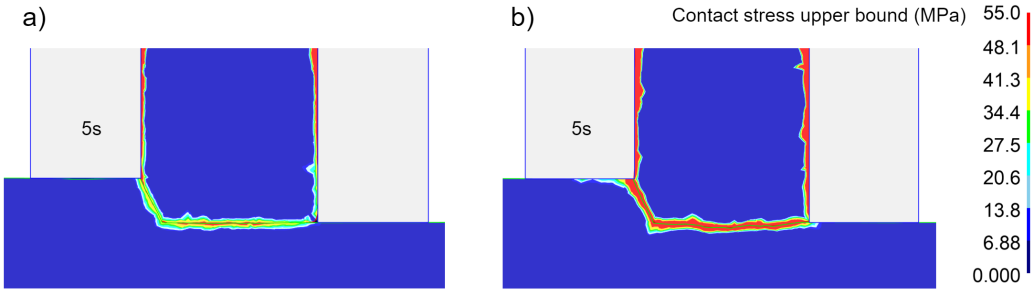


**Figure 15.** Normal pressure in a section through the die transverse to the feed direction. (**a**) balanced speed ratio; (**b**) high speed ratio, 20% over-extrusion.

## 5. Discussion

Through the simulations presented herein, new knowledge and understanding of the HYB-AM process have been gained. These new insights will be valuable in the further development and industrialization of the process.

For the pressure-generating mechanism, it is observed that the strain rates in the plastic zone increase at high rotational speeds. However, the temperatures also increase as a result of (adiabatic) heating due to deformation work. This temperature increase, in turn, reduces the flow stress of the material, and, despite the higher strain-rate, the length of the extrusion grip zone remains virtually unchanged. Furthermore, from the provided results, it is clear that there is no significant increase in contact pressures at higher deposition rates. This means that future experiments can utilize higher flow rates without putting excessive loads on the extruder.

Moreover, it is of interest to observe that the wheel diameter; i.e., the length of the Conform slot can be considered sufficiently long for any extrusion speed. Still, the current extruder design has a limitation in the maximum allowable flow rate due to high peak temperatures in the plastic zone. The simulations show that the temperature increases from the initial pre-heating temperature of 300 °C up to 550 °C in the plastic zone.

From model 1, it is seen how the extrusion grip zone is established. When using feedstock material with a smaller cross-sectional area than that of the groove, the length of the extrusion grip zone will vary depending on the extrusion pressure. A change in the conditions at the die outlet will call for a change in pressure, and, thus, the extrusion grip length will have to adapt accordingly. Since the feedstock material is supplied at a constant speed, the flow rate out of the die will be subjected to reduced flow while the extrusion grip length is increased. This implies that the process is vulnerable to fluctuations in the flow rate and pressures. However, by filling the entire cross-section in the grip zone by means of a coining wheel, the process will respond better to changes in pressures. This can also be beneficial in terms of reduced heat generation, as the slip in the extrusion grip zone will be reduced similarly.

The aim of the simulations carried out in this study has been to analyse and interpret some of the governing mechanisms of the process that are difficult to observe through physical experiments. The relationships between FEA and full-scale experiments for the CRE process have previously been validated through numerous studies by others. Hence, these results provide reliable input for the further process development. For the bonding interface between the extrudate and the substrate, future experiments need to be conducted to further validate the results. However, when briefly comparing to the observations from the prior full-scale experiments, it was observed that the material deposition sequence has been modelled adequately. Figure 16 represents a section of the sample depicted in Figure 2b and is included for reference. This sample was deposited at a rotational speed of 4 RPM and the same feed speed as that used in the simulations presented. For the first stringer, the volumetric flow was set at a level corresponding to that of the high ratio, whereas a balanced ratio was used for the subsequent stringers. Defects in the form of cracks and pores are visible on this sample and indicate substandard bond quality. The FEA results clearly show the importance of using a correct deposition rate vs. feed speed. If the extruder fails to deliver the correct volumetric flow, the contact pressure at the interface will drop below the bonding threshold, resulting in substandard samples. From the simulations, it is also visible that a 'gas-pocket' is formed inside the die in this case. When the scraped surface of the substrate is exposed to the conditions inside this pocket, a new oxide layer can be formed, thus reducing the layer bonding quality.

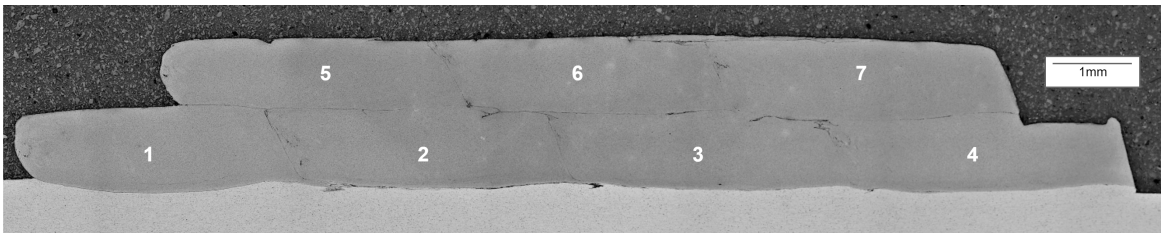


**Figure 16.** Section through the sample shown in Figure 2b with deposition order of the individual stringers indicated. The structure is almost fully dense, yet some pores and areas with lack of bonding are present.

## 6. Conclusions

Based on the FEA results obtained in this study, the following conclusion can be made for the pressure-generating mechanism:

1. Increased angular velocity of the wheel both increases the strain rates and the heat generation due to the higher deformation work.
2. The simulations show that the contact pressure inside the plastic zone is virtually similar at 4 RPM and 50 RPM. For the current design, the maximum deposition rate will be 1 kg/h when the extruder, as well as the substrate material, is pre-heated to 300 °C.
3. The length of the extrusion grip zone is not affected by an increased deposition rate.

Furthermore, from interpretations of the FEA models for the bonding interface between the substrate and the extrudate, the following conclusions can be drawn:

4. In order to obtain sufficient contact pressure for bonding to occur across the full stringer width, the input flow rate needs to be higher than the actual flow out of the rear opening of the die.
5. When the feed speed becomes too high relative to the material flow through the die, a gas pocket is formed in the outlet. This gas pocket can cause oxidation of the scraped surface with reduced bonding quality as a consequence.

**Author Contributions:** Formal analysis, J.B.; Methodology, J.B. and T.W.; Project administration, M.S.; Supervision, T.W. and M.S.; Visualization, J.B.; Writing—original draft, J.B., T.W. and M.S.

**Funding:** This research was funded by the KPN project Value, sponsored by the Research Council of Norway, Hydro and Alcoa.

**Acknowledgments:** The authors acknowledge the support from NAPIC (NTNU Aluminium Product Innovation Center). They are also indebted to Henry Valberg for valuable assistance.

**Conflicts of Interest:** The authors declare no conflict of interest.

## Abbreviations

The following abbreviations are used in this manuscript:

| | |
|---|---|
| AM | Additive Manufacturing |
| CRE | Continuous Rotary Extrusion |
| FEM | Finite Element Method |
| FEA | Finite Element Analysis |

## References

1. Blindheim, J.; Grong, Ø.; Aakenes, U.R.; Welo, T.; Steinert, M. Hybrid Metal Extrusion & Bonding (HYB)—A new technology for solid-state additive manufacturing of aluminium components. *Procedia Manuf.* **2018**, *26*, 782–789. [CrossRef]
2. Blindheim, J.; Welo, T.; Steinert, M. Rapid prototyping and physical modelling in the development of a new additive manufacturing process for aluminium alloys. *Procedia Manuf.* **2019**, *34*, 489–496. [CrossRef]

3. Blindheim, J.; Welo, T.; Steinert, M. First demonstration of a new additive manufacturing process based on metal extrusion and solid-state bonding. *Int. J. Adv. Manuf. Tech.* **2019**, under review.
4. Blindheim, J.; Grong, Ø.; Welo, T.; Steinert, M. On the mechanical integrity of AA6082 3D structures deposited by hybrid metal extrusion & bonding additive manufacturing. *J. Mater. Process. Technol.* **2019**, under review.
5. Green, D. Continuous extrusion-forming of wire sections. *J. INST MET* **1972**, *100*, 295–300.
6. Etherington, C. Conform—A new concept for the continuous extrusion forming of metals. *J. Eng. Ind.* **1974**, *96*, 893–900. [CrossRef]
7. Song, L.; Yuan, Y.; Yin, Z. Microstructural Evolution in Cu-Mg Alloy Processed by Conform. *Int. J. Nonferrous Metall.* **2013**, *2*, 100–105. [CrossRef]
8. Thomas, B.M.; Derguti, F.; Jackson, M. Continuous extrusion of a commercially pure titanium powder via the Conform process. *Mater. Sci. Technol.* **2017**, *33*, 899–903. [CrossRef]
9. Mitka, M.; Misiolek, W.Z.; Lech-Grega, M.; Gawlik, M.; Bigaj, M.; Szymanski, W. Continuous rotary extrusion of magnesium alloy AZ 91. In Proceedings of the Conference: Materials Science & Technology 2015, Columbus, OH, USA, 4–8 October 2015; p. 7.
10. Mitka, M.; Gawlik, M.; Bigaj, M.; Szymanski, W. Continuous Rotary Extrusion (CRE) of Flat Sections from 6063 Alloy. *Key Eng. Mater.* **2015**, *641*, 183–189. [CrossRef]
11. Ji, X.; Zhang, H.; Luo, S.; Jiang, F.; Fu, D. Microstructures and properties of Al–Mg–SI alloy overhead conductor by horizontal continuous casting and continuous extrusion forming process. *Mater. Sci. Eng. A* **2016**, *649*, 128–134. [CrossRef]
12. Kim, Y.H.; Cho, J.R.; Jeong, H.S.; Kim, K.S.; Yoon, S.S. A study on optimal design for CONFORM process. *J. Mater. Process. Technol.* **1998**, *80*, 671–675. [CrossRef]
13. Hodek, J.; Zemko, M. FEM Model of Continuous Extrusion of Titanium in DEFORM Software. In Proceedings of the 2nd International Conference on Recent Trends in Structural Materials, Parkhotel Plzen, Czech Republic, 21–22 November 2012; p. 7. Available online: http://comat2014.tanger.cz/files/proceedings/11/reports/1326.pdf (accessed on 5 May 2019).
14. Valberg, H.; Rajendran, N.; Misiolek, W. The Mechanics of the Continuous Rotary Extrusion Process Investigated by FEM analysis. In Proceedings of the Eighth International Conference On Advances in Mechanical, Aeronautical and Production Techniques-MAPT 2018, Kuala Lumpur, Malaysia, 3–4 February 2018; pp. 1–7. [CrossRef]
15. Rajendran, N.; Valberg, H.; Misiolek, W.Z. The FEM simulation of continuous rotary extrusion (CRE) of aluminum alloy AA3003. *Aip Conf. Proc.* **2017**, 050004. [CrossRef]
16. Rajendran, N.; Mitka, M.; Lech-Grega, M.; Misiolek, W.Z. Effect of tool geometry on the velocity and strain rate fields in continuous rotary extrusion of magnesium AZ91 alloy. *Procedia Manuf.* **2018**, *15*, 264–271. [CrossRef]
17. Akeret, R. Extrusion welds-quality aspects are now center stage. In Proceedings of the 5th International Aluminium Extrusion Technology Seminar, Chicago, IL, USA, 19–22 May 1992.
18. Valberg, H. Extrusion welding in aluminium extrusion. *Int. J. Mater. Prod. Technol.* **2002**, *17*, 497–556. [CrossRef]
19. Yu, J.; Zhao, G. Interfacial structure and bonding mechanism of weld seams during porthole die extrusion of aluminum alloy profiles. *Mater. Charact.* **2018**, *138*, 56–66. [CrossRef]
20. Yu, J.; Zhao, G.; Chen, L. Analysis of longitudinal weld seam defects and investigation of solid-state bonding criteria in porthole die extrusion process of aluminum alloy profiles. *J. Mater. Process. Technol.* **2016**, *237*, 31–47. [CrossRef]
21. Heinemann, H. Flow Stress of Different Aluminum and Copper Alloys for High Strain Rates and Temperature. Ph.D. Thesis, TH Aachen, Aachen, Germany, 1961.
22. Valberg, H.S. *Applied Metal Forming*; Cambridge University Press: Cambridge, UK, 2006.